A COMPUTATIONAL MODEL FOR THE PREDICTION
OF NET POWER IN PROTON EXCHANGE MEMBRANE FUEL CELLS

*Nima Norouzi[1], Saeed Talebi[1, *]*

Abstract. This paper aims to quantify the rate of improvement of electrical energy due to oxygen enrichment. For a specific membrane effective area (MEA), the flow field (FF) designer is always ready to design the FF to maximize the amount of oxygen in all areas of the catalyst layer (CL). Using the guidelines in this paper, FF designers, without cumulative computational fluid dynamics (CFD) calculations, can predict the rate of electrical energy gain due to 1 % enrichment in the amount of oxygen present in the CL. A 3D CFD tool was used to answer this question. These three constant steps of the reaction product simulate the humidified air mixture at the proton exchange membrane fuel cell (PEMFC). Results show that the analytic methods and the dynamic computational method introduced in this paper are similar in results, and the error of the CFD model is about 1.9 % compared to the analytic method.

Keywords: computational fluid dynamics, flow field design, fuel cell, performance analysis.

1. Introduction

Fuel cells are the future energy source, and the proton membrane exchange (PEMFC) is one of the most important clean energy generators for mobile, mobile, and fixed applications. PEMFCs have zero to zero emissions, can operate at low temperatures, provide high energy density, and have a rapid start.[1-5] It is necessary to design and optimize fuel cells for better performance and efficiency.[6-10] Field design in dipole plates is one of the main parameters of the catalyst layers electronic use (CL).

PEMFC acts as a resource for collectors and products. The reagents, as well as the products, are transported to the cell through the flow channels. Properly designed design can improve reaction and remove the product from the cell. This reduces concentration losses, which generally occur at a high current density.[1,3] The dipole plate is an essential component of fuel cells that can occupy up to 80 % by weight and about 50 % of the total cell cost.[11]FF designers goal is to maximize the content of reactive species in all regions of the catalyst layer (CL). The FF designer in the fuel cell is designed with a better FF design than the catalyst layer (CL).[11-13]Tehlar*et al.*[14] developed a model to examine the different geometry of channel sides andgas diffusion layer (GDL) characteristics. The results showed that the cross thermal load could increase the current density and, thus, the cell energy density. Severe sensitivity to pressure, speed, and speed of gears were observed. As an exceptional value, the thickness of the GDL under gear increases, increasing the current density by approximately 20 %. Detailed knowledge of GDL features is important for the understanding of channel load and performance improvement. Wang *et al.*[15] developed a general template for the interior maps of the most popular U-shaped designs, including types of spiral, multi-loop, parallel, straight, and interlocking structures. The flow distribution and the pressure drop in the multiple serpentines were between the straight parallel and the single serpentine. It provides practical guidelines for assessing fuel cells progress by designing operating conditions and measuring how to improve flow distribution and pressure drop.[15] Liu *et al.*[16] studied and designed tapered channels designed to reduce PEMFC flow fields. By reducing the channel cross-sectional area, the oxygen transfer to the gas distribution layer will be more effortless while the oxygen content decreases due to the cathode reaction, thereby increasing cell performance. The results also show that the effect of liquid water

[1] Department of Energy Engineering and Physics,
Amirkabir University of Technology (Tehran Polytechnic),
424 Hafez Ave., PO Box 15875-4413, Tehran, Iran
[*] *sa.talebi@aut.ac.ir*

generally affects cell performance. Ramesh *et al.*[17] study the different channel sizes and channel sizes for the parallel PEMFC field to ensure uniform distribution of fuel and oxygen at reaction sites. The channel width varies from 0.5 to 2 mm, and the gear size varies from 0.2 to 1.2 mm. The results showed decreased cellular function as the gear size increased, but the increased channel width improved the cellular function.[17] By classifying the fuel cell CFD solvent, two different methods for evaluating cell performance can be explored.Method 1: Distribution of ponds/fixed sources in the catalyst layers. In this CFD method, the equations that govern the fluid are solved, for example, in the cathode electrode fraction (Y_{O2}) CL in the CL/GDL interface, which is evaluated as part of the solution. In general, the higher the value of CL (Y_{O2}), the better the cell performance. However, like this method, the current-voltage relationship is not used, and the cell density, voltage, and current energy density are not evaluated. Therefore, cell performance (such as cell energy density) can qualitatively match higher CL (Y_{O2}) with higher cell energy density. Method 2: Variable sink/source distribution in the catalyst layer. In this CFD method, in addition to equations that control fluid motion, the voltage-current flow (group ratio) is also solved with the cell. Therefore, in addition to CL (Y_{O2}), the cell current density and energy density can be calculated for the specified cell voltage. This approach (method 2) allows a quantitative relationship between the increases in cellular energy density due to the increase in the percentage of units in (Y_{O2}) CL. This is in contrast to the approach that can only lead to qualitative results. This study aims to determine the rate of improvement of electrical energy (or energy density) due to enrichment in the oxygen content or, for example, part of the oxygen mole when exposed to CL. As mentioned before, the CFD method is used in this study. The ANSYS® FLUENT® commercial software package was used for this purpose. The present study investigates the membrane-effective area's performance, the cell-specific operating conditions, and direct parallelism. This approach can be further expanded. In this document, nine different geometries of the channels with G_1 to G_9 are represented (see Figs. 1 and 2). The active cell region was identical in all cases. The contrast of the oxygen molecule fraction is observed in the benzene layer (GDL) and the catalyst layer interface (CL), (Y_{O2}) CL. In studying numerical data, a relationship was established between MEA and net

power density. For the cases investigated, the current model provides a basis for predicting the electrical energy generated (P_g) and pure energy (P_{net}) by knowing only a portion of the oxygen molecule versus the catalyst layer and the origin and its effect of low voltages is important.[16] And also, one of the purposes of this work is to determine the increase in net strength due to oxygen enrichment in CL.

2. Experimental

In this paper, computational fluid dynamics (CFD) is being implemented to model a PEM fuel cell. The CFD is a rapidly developing science and field of numerical solving of fluid mechanics problems. This method is used to create quantitative predictions and analysis of the fluid flow. Suppose the process is developed correctly and assumptions are made appropriately in the system. In that case, it will be an ideal solution for complex parametric studies and flow-physics or flow-chemistry researches that otherwise would be impossible or impractical to be analytically solved or modeled. Two different approaches of the CFD are finite-differences and finite-volume or element formulations. In both approaches method uses discretizing the spatial domain into a grid or mesh of point elements and marching the numerical solution forward into discrete time steps. In the finite-difference formulation, individual derivative terms in the motion equations are written in terms of field-value differences determined at or between the grid of mesh states, and the output system of mathematical equations is solved numerically. In the finite volume or element formulation, the equations of motion are solved within small elements whose sum covers the entire system (the spatial domain of the system), and this model leads to an algebraic system of equations that are solved numerically. In this paper, the second approach is used and modeled in the following equations.

For a cell with MEA and stable operating conditions, Y_{O2} can be increased with many different background changes in Florida AH (FF). For example, increased channel-to-gear ratio (w/d); lower channel height (h); increased mass flow through channels (m); techniques that increase over-rib-convections,*etc*. In all investigated cases, the pumping power changes and the netpower (P_{net})

should be considered in place of the only power produced by the cell, which is formulated by the following equations:[14]

$$P_{net} = i \cdot V_{cell} - \Delta P \frac{V}{A} \qquad (1)$$

$$P_g - i.V_{cell} = 0 \qquad (2)$$

$$P_{pump} - \mathrm{D}P.\frac{V}{A} = 0 \qquad (3)$$

The first term in Eq. (1) shows the produced power. Besides, the term II is the pumping force, where ΔP is the pressure drop across the flow channel, the mean medium volume is low, and the cell's active region. The balance between conditions I and II provides the net energy that the P_{net} cell generates. P_g is the cell's energy density determined by the current density of cell i and the cell voltage V_{cell}. It has been shown by Liu *et al.*[18] that "with high utilization, to transfer 50 % for 1% fertilization in Y_{O2} within CL, 0.3 to 0.4 % in energy density is expected".P_g and P_{net} provide the catalyst by calculating only the molar portion of oxygen on the cathode layer's face.This relationship is obtained using numerical data and analytical approximation and discussed at the end of the section.

The computational field consists of one L channel, connected at the top with a layer of diesel gas (GDL) where the layer (CL) is located. Fig. 1 shows the field maps. Numerical simulations of the different geometry of gas channels in the fixed region of the Middle East and Africa (fixed region of the cell) are performed to determine the relationship between the cell's net power density and the molecular oxygen part. Therefore,nine geometries (from G_1 to G_9) are used in Table 3 for this element as the studied intervals. Generally speaking, a flow field geometrical parameters can be defined using channel width, height, and length, respectively w, h, and$L$, and the ribs between two adjacent channels, d. Previous

studies[19,20] found that the following ranges were considered for channel parameters, sides, and channel width above channel depth and gear channel width.
- Channel width (w), $0.4 \leq w \leq 1.0$ mm
- Rib width (d), 0.6 mm $\leq d$
- Channel width divided than channel depth (w/h), $w/h > 0.7$
- Channel width divided by rib width (w/d), $w/d > 0.4$

Numeric values of G_1 to G_9 are shown in Table 3, and network independence was evaluated using the formulation. The appropriate network sizes used in this study are reported in Table 1. All simulations are performed after MEA (membrane-effective area). Repeated unit size width fixed (channel width with rib$d$) is 1.5 mm. The governing equations (described in subsection 2.1) are solved using the ANSYS® FLUENT® software package scientific version. The TOEFL equation, described in subsection 2.1, has been combined as a function (UDF) in the software environment to voltage-to-connect (v-to-c). The physical properties and operating conditions used in the current calculations are presented in Table 2.
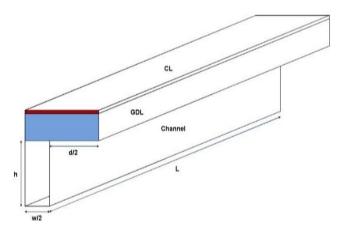

Fig. 1. Schematic of the domain of the computation

Table 1. Dimensions and meshes of the computational domain for a sample case G-1

Zone	Length (mm)/mesh	Width (mm)/mesh	Height (mm)/mesh	Rib width (mm)/mesh
Flow channel	80/300	0.5/10	0.4/10	1/20
Gas diffusion layer	80/300	1.5/30	0.25/7	–
Catalyst layer	80/300	1.5/30	0.025/4	–

Table 2. Physical properties and operating conditions used in the present computation

Parameter	Value
Open circuit voltage (VO.C.)	1.09 V
Cell voltage (V_{cell})	0.2, 0.3, 0.5, 0.6 V
Operating temperature (T)	327K
Operating pressure (P)	101000 Pa
Faraday constant (F)	96500 C/mol
Gas constant (R)	8.314 J/mol·K
Dew point temperature ($T_{dew\ point}$)	311 K
Utilization (u)	50%
The porosity of the gas diffusion layer, ε_{GDL}	0.71
Fluid viscous resistance of the gas diffusion layer($1/K$)	$5.6 \cdot 10^{10} 1/m^2$
The porosity of the catalyst layer, ε_{CL}	0.72
Area-specific resistance (σ)	$1.05 \cdot 10^{-5} \Omega \cdot cm^2$
Charge transfer coefficient (α_C)	0.52

2.1. Model Assumptions

The following was assumed:

• due to the cathode importance as a limiting component of PEM fuel cells performance, only the cathode side is considered;

• system operates under steady conditions;

• it is a single phase;

• the mixture is incompressible;

• flow is regarded as a laminar;

• the gravitational effects are ignored, and the flow is driven solely because of the pressure gradient;

• the used layer of the gas and the catalyst layer are treated as homogeneous isotropic porous materials.

The governing equations for the channel (as a clear region) and the differential gas and catalyst layers are written in a unified model, where the equations contain porosity (ε) and permeability values (K). The channel areaε is set to 1 and $K \to \infty$, and in the GDL and CL regions, the values specified in Table 2 are used for K and ε. To maintain mass for a gas mixture of three species (Eq. 4):

$$\frac{\partial(\varepsilon\rho)}{\partial t} + \nabla \cdot (\varepsilon\rho\vec{V}) = Sm \tag{4}$$

where ε is porosity, ρ is density, t is time, $\vec{V}$ is the velocity vector, and S_m is the source of the mixed term, which is defined later in this section. The mixture momentum equation in the canal region is calculated byEq.(5):

$$\frac{\partial(\rho\vec{V})}{\partial t} + \nabla \cdot (\rho V\vec{V}) = \nabla P + \nabla \cdot (\mu\nabla\vec{V}) \tag{5}$$

In Eq.(6), the value of$P$is gravitational pressure, and μ is the fluid velocity. The equation of momentum in the porous areas of GDL and CL is defined using Darcy's law (Eqs. 6 and 7):

$$e\overset{ur}{V} = - \frac{k}{m}\tilde{N}P \tag{6}$$

The mixture energy equation is:

$$\frac{\partial(\varepsilon\rho CpT)}{\partial t} + \nabla \cdot (\varepsilon\rho CpT\vec{V}) = \nabla \cdot (k^{eff}\nabla T) \tag{7}$$

T is the temperature, C_P is the specific heat at constant pressure, and $k_{eff}$is the effective heat transfer coefficient. Species transport equations using Fick's law are written as follows (Eq. (8)):

$$\frac{\partial(\varepsilon Ci)}{\partial t} + \nabla \cdot (\varepsilon\vec{V}Ci) = \nabla \cdot (Di^{eff}\nabla Ci) + Si \tag{8}$$

whereS_i is the source term for the species, in which the subtitle i represents O_2 and H_2O.

In-channel and GDL S_i in CL will be specified in this section. The user-defined functionality (UDF) of the ANSYS® FLUENT® software combines the reaction kinetics in the catalyst layer through the TOEFL equation to relate the voltage to current (v-to-c). This method can distribute the local current density i and the sink/source terms in CL. S and i are integrated with Faraday's law as follows. For the cell current density given as$i$ (A/cm^2), the oxygen molecule consumption is(Eq. 9):

$$n_{O_2} = i \cdot \frac{A}{4F} \tag{9}$$

where A is the active region of the cell, and F is the Faraday constant. Accordingly, the amount of oxygen consumption consumed is determined byEq. (10):

$$m_{O_2} = -M_{O_2} i \cdot \frac{A}{4F} \qquad (10)$$

where M_{O2} is the molecular weight of oxygen. The negative sign in Eq. (10) indicates the amount of oxygen consumed. Hence, the *S*-term of oxygen:

$$S_{O2} = \frac{m_{O2}}{(vol)_{cl}} \qquad (11)$$

where $(vol)_{CL}$ is the volume of CL. Therefore:

$$S_{O_2} = -M_{O_2} i \cdot \frac{A}{4F} \cdot \frac{1}{(vol)cl} \qquad (12)$$

Similarly to O_2, the molar water vapor is related to the rate of n_{H2O} (Eqs. 13-15):

$$n_{H2O} = i \cdot \frac{A}{2F} \qquad (13)$$

$$S_{H2O} = i \cdot \frac{A}{2F} \cdot \frac{1}{(vol)cl} \qquad (14)$$

$$S_m = S_{H2O} + S_{O2} \qquad (15)$$

The current-voltage relationship is established using the TOEFL and applied to the UDF code:

$$h = \frac{RT}{a \, cF} \ln(\frac{iCo_2{}^{ref}}{i_0 Co_2}) \qquad (16)$$

where i_0 is the current exchange density, $C^{ref}{}_{O2}$ is the reference oxygen mass transfer, and α_C is the cathode charge transfer inhibition. Therefore, the cell voltage can be obtained from:

$$V_{cell} = V_{ref} - h - s_i \qquad (17)$$

where σ is the overall cell resistance, including the membrane protons, resistance, and the electronic resistance of GDL and other parts of the cell, to assess the solution dependence on network size, the network independence was investigated. Table 1[21] lists the appropriate grid sizes used in the current method.[22,23]

3. Results and Discussion

Fig. 2 shows the comparison between the current calculations for polarization curve and experimental data obtained by other researches.[20,24] As shown in the figure, there is an acceptable agreement between the data. Since the verification parameters differ from those used in the current method (Table 2), the physical properties in the present calculations are modified for verification purposes, *i.e.,T* = 351 K, *P* = 101000 Pa, the input speed is 0.41 m. Second, the inlet's relative humidity is 10 %, and the monophasic mixture of water vapor and oxygen is considered following the data listed in Tables 1 and 2.

This document describes optimal channel calculations for a PEM fuel cell. The primary purpose of this paper is to establish the relationship between net cell density (P_{net}) and an average molar portion of oxygen (Y_{O2}) *versus* cathode reaction (GDL/CL interface). Channels with different dimensions for different cross-sections (see Table 3) are analyzed to capture the baseline relationship. Fig. 3 shows an example of mathematical results for geometric elements 1 to 9 (G_1 to G_9). The red line diagrams illustrate the polarization curve.[23] As expected, the current density increases with the decrease in cell voltage. Fig. 4 analyzes the comparison of the polarization curves of G_1–G_9. Greenline graphs show changes in the mol-oxygen portion with the current cell density. This graph shows the oxygen content on a PEM fuel cell's cathode side compared to the polarization curve. The blue line diagrams show changes in the electrical energy density caused by the current cell density. The diagram is approximately linear up to $i = 1$ A/cm^2. Note that numerical calculations are performed with a cell voltage from 0.2 to 0.65 V, so the graphs show the calculated range as a part of the functional cell voltage (*i.e.*, from 0 to 1.1 V).[22,25]
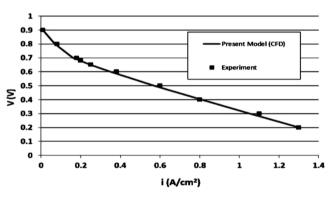

Fig. 2. Comparison between the polarization curve for the calculated results and experimental data[20,24]

The change in the molecular part of oxygen shows the current cell density. This graph shows the oxygen content on a PEM fuel cell's cathode side compared to the polarization curve. The blue line diagrams show changes in the electrical energy density caused by the current cell density. The graph is approximately linear up to $i = 1$ A/cm^2. Note that the numerical calculations are performed with a cell voltage of 0.2–0.65 V.

Consequently, the graphs show the calculated range as part of the total operating cell voltage (*i.e.*, from 0 to 1.1 V). Fig. 4 shows a comparison of the polarization curves of G_1 with G_9. As shown in this case, the difference between the polarization curves occurs in regions with low oxygen concentration (high current

density or low cell voltage), where focus losses play an important role. Table 3 shows the contribution of each of the essential components of the loss to the fuel cell, namely activation, resistance, and concentration.

Changing the geometry of the gas channel leads to changes in the mass transfer mechanisms. Therefore, focus losses are reduced in channels with the appropriate geometry.
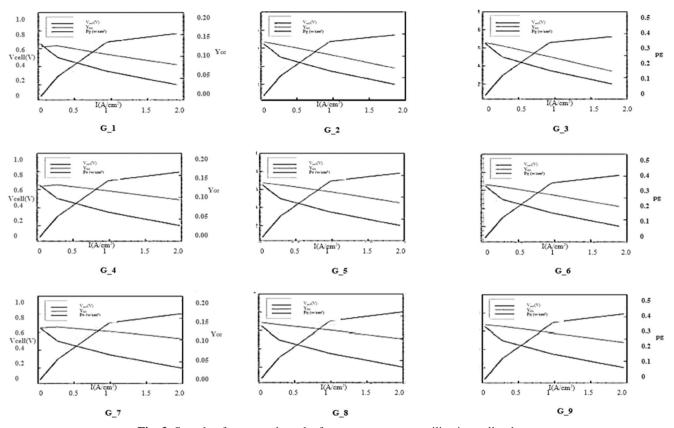

Fig. 3. Sample of computed results for constant oxygen utilization,cell voltage, and generated power density with current cell density (at I = 0, P_{net} has the lowest and Y_{O2} has the highest V_{cell})
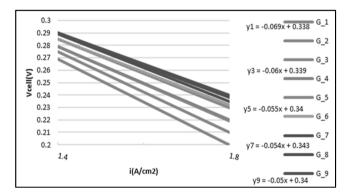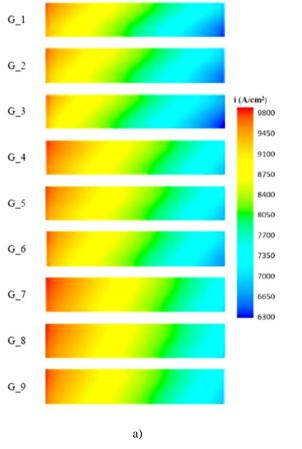

Fig. 4. Comparison of the polarization curves for cases G_1 – G_9 and constant oxygen utilization in low concentration region (G_9 is the highest and G_1 is the lowest)

On the other hand, by increasing cellular voltages (or reducing current density), the probability of losing

focus is low. Therefore, channel engineering changes occur in areas with low current density. This can be explained using a variety of terms. In areas with low current density, oxygen consumption is low. Therefore, oxygen will have sufficient time to reach the reaction sites within the CL.

In contrast, in areas with high current density, oxygen consumption is high. Therefore, the reaction constraint can be oxygen. Better oxygen supply to the reaction can be achieved to reduce these conditions using appropriate channel engineering. Fig. 5 shows the oxygen molecular fracture lines at the GDL/CL interface for all cases (G_1–G_9) for oxygen use and $V = 0.35$ V. The channel width for G_1–G_3 is 0.5 mm, for G_4–G_6 is 0.7 mm, and for G_7–G_9 is 0.9 mm for active region control volume. Fig. 6b shows that channels with a larger

channel width contain more oxygen compared to the catalytic layer (GDL/CL interface). Fig. 6a shows the current density lines in the GDL/CL interface for all cases for the tight use of oxygen and $V = 0.35$ V. Figs. 6a and 6b show that Y_{O2} is directly proportional the quantity produced and the channel width is more abundant in oxygen within the CL. The results shown in Fig. 6 are obtained based on physical properties. Operating conditions are given in Table 2 using the cell voltage of 50 % and 100 % of the maximum possible value. The calculation time for all states (G_1 to G_9) is summarized with V_{cell} values of 0.2, 0.35, 0.5, and 0.65 V. This table indicates the use of 50 wt % of conventional oxygen and contains 14 parameters (Table 3 calculates results using 50 wt % of oxygen). The cell mass and density are estimated experimentally. As reported in Table 3, an increase in Y_{O2}@GDL/CL is being detected. The reason is that the Y_{O2}@GDL/CL is the delivery time for the reaction kinetics in the CL, and the higher the Y_{O2}@GD

/CL,the higher the reaction kinetics in CL. Table 3 shows that it is more important for higher mass and cross-sectional areas with a lower channel.
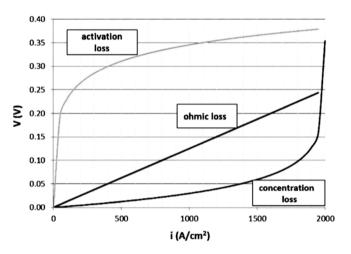

Fig. 5. Schematic contributions of the loss components from activation-, ohmic- and concentration-losses
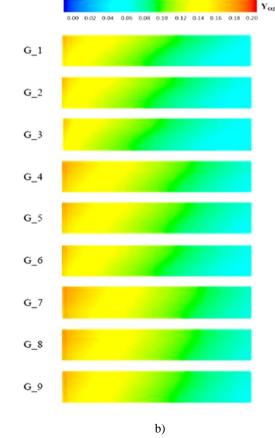

a)   b)

Fig. 6. The contour of current density (a) and oxygen mole fraction (b) at GDL/CL interfaces for constant oxygen utilization and $V= 0.35$ V

Table 3. Summary of the simulation results for cases G_1–G_9

Case	m·e+7, kg/s	i, A/cm^2	V_{cell}, V	u	ΔP, kPa	$\Delta P/L$, kPa/m	Y_{O2}	P_{pump}, W/cm^2	P_g, W/cm^2	P_{net}, W/cm^2
G_1	8.3496	1.86445	0.196	0.49	1.51948	18.99338	0.079331	0.002097	0.37289	0.370793
	4.165	0.930216	0.343	0.49	0.8935934	11.17004	0.102214	0.000617	0.325576	0.324958
	1.1956	0.26607	0.49	0.49	0.2776242	3.47018	0.121481	5.88E-05	0.133035	0.132976
	0.1372	0.029596	0.637	0.49	0.3485664	4.35708	0.119893	9.8E-06	0.019237	0.019228
G_2	8.1144	1.812412	0.196	0.49	0.6815704	8.52012	0.070707	0.000921	0.362482	0.361571
	4.1552	0.928648	0.343	0.49	0.343931	4.29926	0.101273	0.000235	0.325027	0.324792
	1.1956	0.267932	0.49	0.49	0.1137192	1.421	0.122539	1.96E-05	0.133966	0.133946
	0.1372	0.031654	0.637	0.49	0.034692	0.43414	0.129507	0	0.02058	0.02057
G_3	7.84	1.751064	0.196	0.49	0.4167156	5.2087	0.062857	0.000539	0.350213	0.349674
	4.067	0.90846	0.343	0.49	0.2142084	2.67736	0.095432	0.000147	0.317961	0.317814
	1.1858	0.263816	0.49	0.49	0.0701484	0.8771	0.119854	9.8E-06	0.131908	0.131898
	0.1372	0.031164	0.637	0.49	0.0345058	0.4312	0.127116	0	0.020257	0.020257
G_4	8.6534	1.930796	0.196	0.49	0.898709	11.23374	0.092051	0.001284	0.386159	0.384875
	4.3022	0.961576	0.343	0.49	0.400281	5.00388	0.112043	0.000284	0.336552	0.336267
	1.2152	0.27146	0.49	0.49	0.0846328	1.05742	0.125812	1.96E-05	0.13573	0.13571
	0.1372	0.029988	0.637	0.49	0.202713	2.53428	0.121853	0	0.019492	0.019492
G_5	8.4966	1.8963	0.196	0.49	0.3646482	4.55798	0.085093	0.00051	0.37926	0.37875
	4.2826	0.95697	0.343	0.49	0.1626898	2.0335	0.110152	0.000118	0.334944	0.334827
	1.2152	0.271264	0.49	0.49	0.0616028	0.77028	0.125264	9.8E-06	0.135632	0.135622
	0.147	0.03185	0.637	0.49	0.0119658	0.14994	0.130183	0	0.020707	0.020698
G_6	8.3104	1.85612	0.196	0.49	0.196098	2.45098	0.07891	0.000274	0.371224	0.37095
	4.214	0.94129	0.343	0.49	0.104321	1.30438	0.105174	6.86E-05	0.329456	0.329378
	1.2054	0.268324	0.49	0.49	0.033516	0.41846	0.123215	9.8E-06	0.134162	0.134152
	0.1372	0.03136	0.637	0.49	0.0155722	0.19502	0.127851	0	0.020384	0.020384

Note that the mass through the channels is the main parameter in the pressure drop. In each calculated case, 50 % of usage and the given value of V_{cell} will be compensated. The smallest V_{cell} values correspond to more significant pressure differences and larger flow based on the polarization curve. $\Delta P/L$ shows the pressure gradient along the channel. This parameter explains the operating fluid's ability to arrange the condenser toward the channel outlet and avoid waste.[20,21] The value of P_{pump} shows the pumping force needed to carry the work through the channel. P_{pump} is determined from $\Delta PV/A$, where V and A are the average volumetric flow rates in the channel and the active cell area, respectively, and the ΔP is the pressure difference. P_g represents the fuel cell energy density ($P_g = i \cdot V_{cell}$), and the P_{net} parameter is the cell net

energy density, calculated from Eq. (1). Fig. 7 shows the pressure gradient value for all states (G_1 to G_9) in kPa/m, proportional to 0.2, 0.35, 0.5, and 0.65 V of cellular voltage and continuous oxygen use. The small pressure gradient keeps the remaining liquid water inside the channel, reducing the cell confidence level. Therefore, it is recommended to check for pressure drop along the channel. The minimum for all calculated ranges is 2 kPa/m. High-pressure gradients lead to increased pumping energy and erratic pressure distribution in the MEA. Therefore, the upper limit for the entire calculation area is 20 kPa/m.[21-24] Cases with a pressure gradient drawn between two parallel lines are considered acceptable cases. The following figure illustrates the first step in selecting acceptable data.
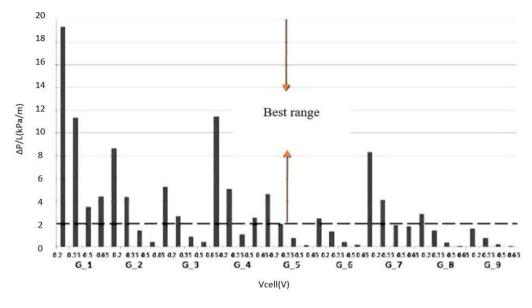
Fig. 7. Pressuregradient amount for all cases in kPa/m and proportional to cell voltage 0.2, 0.35, 0.5, and 0.65 V of the constant utilization

Two parallel lines drawn are considered to be the case. The following diagrams show the first step in reducing calculation costs. Eqs.(18)–(22) show the net power density changes with the oxygen mole fraction in the face of the GDL/CL interface at operating voltages of 0.2–0.65 V for G_1–G_9 cases. As shown in this graph, this change is linear, and the equations are as follows:

$$P_{net} = 1.132Y_{O_2} + 0.321 \tag{18}$$
$$P_{net} = 1.141Y_{O_2} + 0.311 \tag{19}$$

$$P_{net} = 0.739Y_{O_2} + 0.077 \tag{20}$$
$$P_{net} = 1.121Y_{O_2} + 0.001 \tag{21}$$

General form can be considered as:

$$P_{net} = a \cdot Y_{O_2} + b \tag{22}$$

For any channel geometry, in a specific operating voltage and a simple and fast numerical simulation with fixed sink and source in CL, using the diagram given in Fig. 8 and Eqs. (18)–(22), the cell netpower density wouldbe calculated. The procedure is described in Fig. 8.
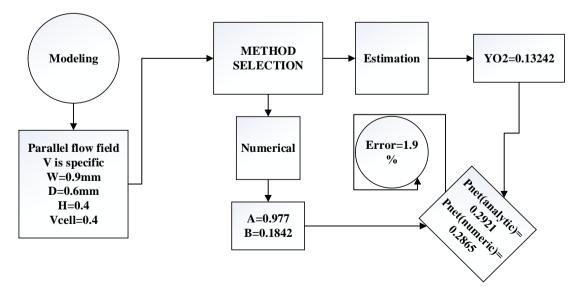

Fig. 8. Comparing analytical and numerical (CFD) net power density calculation methods

Table 4. The statistical accuracy of the model compared to the experimental values

State	RMSE	SSE	MSA	MAE
G_1	0.981242218	0.932180107	0.912555263	0.784993775
G_2	0.985257938	0.935995041	0.916289883	0.788206351
G_3	0.935291005	0.888526455	0.869820635	0.748232805
G_4	0.973125071	0.924468817	0.905006316	0.778500057
G_5	0.900830578	0.85578905	0.837772438	0.720664463
G_6	0.956235512	0.908423737	0.889299027	0.76498841
G_7	0.928111418	0.881705847	0.863143619	0.742489135
G_8	0.946067294	0.898763928	0.879842583	0.756853835
G_9	0.89689437	0.852049652	0.834111765	0.717515496

The data presented in Table 4 states that the models presented in the form of linear regression are accurate enough to be used in the power estimation in the PEM fuel cells, and using these models makes the energy system equations of the fuel cell simpler and much easier to be solved with an acceptable accuracy ratio.

4. Conclusions

The oxygen mole fraction (Y_{O2}), which indicates the amount of oxygen presence at the reaction site (GDL/CL interface), is higher in areas above the channel than in regions above the ribs. The oxygen content increases with increasing channel width and decreases with increasing rib width. The oxygen mole fraction is directly proportional to the produced current density. Channel-wide items have a higher oxygen content inside the CL, hence providing more electrical current. For all cases considered, it has been observed that for a given cell voltage, the net power density of the cell is linear vs. the oxygen mole fraction (Y_{O2}) of CL. Using the data regression techniques in this paper, one can predict how much electrical energy can be generated due to a 1 % enrichment in oxygen content within the CL. For example, it has been observed that at $V = 0.35$ V, a net power increase of 3.5 % for 1% enrichment in oxygen content happens within the CL.

Acknowledgments

References

[1] Wang, X.-D.; Duan, Y.-Y.; Yan, W.-M.; Peng, X.-F. Local Transport Phenomena and Cell Performance of PEM Fuel Cells with Various Serpentine Flow Field Designs.*J. Power Sources***2008**, *175*, 397-407. https://doi.org/10.1016/j.jpowsour.2007.09.009

[2] Ramesh, P.;Duttagupta, S.P. Effect of Channel Dimensions on Micro PEM Fuel Cell Performance Using 3D Modeling.*Int. J. Renew. Energ. Res.***2013**, *3*, 353-358.

[3] Choghadi, H.;Kermani, M. 10th Int. Conf. on Sustainable Energy Technologies SET2011, September4-7, 2011, Turkey, Istanbul.

[4] Bernardi, D.M.;Verbrugge, M.W. A Mathematical Model of the Solid☐Polymer☐Electrolyte Fuel Cell.*J. Electrochem.* **1992**, *139*, 2477. https://doi.org/10.1149/1.2221251

[5] Khakbaz-Baboli, M.;Kermani, M.J. A Two-Dimensional, Transient, Compressible Isothermal and Two-Phase Model for the Air-Side Electrode of PEM Fuel Cells.*J. Electrochem. Acta***2008**, *53*, 7644-7654. https://doi.org/10.1016/j.electacta.2008.04.017

[6] Okada, O.; Yokoyama, K. Development of Polymer Electrolyte Fuel Cell Cogeneration Systems for Residential Applications. *Fuel Cells***2001**, *1*, 72-77. https://doi.org/10.1002/1615-6854(200105)1:1%3C72::AID-FUCE72%3E3.0.CO;2-P

[7] Thoennes, M.;Busse, A.; Eckstein, L.Forecast of Performance Parameters of Automotive Fuel Cell Systems – Delphi Study Results.*Fuel Cells***2014**, *14*, 781-791. https://doi.org/10.1002/fuce.201400035

[8] Wieser, C.Novel Polymer Electrolyte Membranes for Automotive Applications – Requirements and Benefits.*Fuel Cells***2004**, *4*, 245-250. https://doi.org/10.1002/fuce.200400038

[9] Britz, P.;Zartenar, N.PEM – Fuel Cell System for Residential Applications. *Fuel Cells***2004**, *4*, 269-275. https://doi.org/10.1002/fuce.200400043

[10] Kakati, B.K.; Mohan, V.Development of Low-CostAdvanced Composite Bipolar Plate for Proton Exchange Membrane Fuel

Cell.*Fuel Cells***2008**,*8*, 45-51.
https://doi.org/10.1002/fuce.200700008

[11] Yi, P.Y.; Peng, L.F.; Lai, X.M.; Liu, D.A.; Ni, J. A Novel Design of Wave-Like PEMFC Stack with Undulate MEAs and Perforated Bipolar Plates.*Fuel Cells***2010**,*10*, 111-117.
https://doi.org/10.1002/fuce.200900031

[12] Shamardina, O.;Kulikovsky, A.A.;Chertovich, A.V.; Khokhlov, A.R. A Model for High-Temperature PEM Fuel Cell: The Roleof Transport in theCathodeCatalyst Layer.*Fuel Cells***2012**,*12***,** 577-582. https://doi.org/10.1002/fuce.201100144

[13] Ghanbarian,A.; Kermani, M.J.; Scholta, J. Generalizationof a CFD Model toPredictthe Net Power in PEM Fuel Cells.*Iran. J. Hydrogen Fuel Cell***2019**, *6*, 23-37.
http://doi.org/10.22104/ijhfc.2019.3176.1179

[14] Choi, K.-S.; Kim, B.-G.; Park, K.; Kim, H.M. Current Advances in Polymer Electrolyte Fuel Cells Based on the Promotional Role of Under-rib Convection.*Fuel Cells***2012**,*12***,** 908-938. https://doi.org/10.1002/fuce.201200035

[15] Chapter 1.In *Fluid Mechanics(Fifth Edition)*;Kundu, P.; Cohen, I.; Dowling, D., Eds.; Academic Press, 2012, pp 1-37.
https://doi.org/10.1016/B978-0-12-382100-3.10001-0.

[16] Tehlar, D.;Flückiger,R.;Wokaun, A.;Büchi, F.Investigation of Channel-to-Channel Cross Convection in Serpentine Flow Fields. *Fuel Cells***2010**, *10***,** 1040-1049.
https://doi.org/10.1002/fuce.201000034

[17] Wang, J.; Wang, H.Flow-Field Designs of Bipolar Plates in PEM Fuel Cells: Theory and Applications.*Fuel Cells***2012**, *12*, 989-1003. https://doi.org/10.1002/fuce.201200074

[18] Liu, H.C.; Yan, W.M.; Soong, C.Y.;Chen, F.;Chu, H.-S. Reactant Gas Transport and Cell Performance of Proton Exchange Membrane Fuel Cells with Tapered Flow Field Design.*J. Power Sources***2006**,*158*, 78-87.
https://doi.org/10.1016/j.jpowsour.2005.09.017

[19] Hasmady, S.; Wacker, M.;Fushinobu, K.; Okazaki, K. ASME-JSME Thermal Engineering Summer Heat Transfer Conference, Vancouver, British Columbia, Canada, 2007; 20.

[20] Akhtar, N.;Qureshi, A.;Scholta, J.;Hartnig, C.;Messerschmidt, M.;Lehnert, W. Investigation of Water Droplet Kinetics and Optimization of Channel Geometry for PEM Fuel Cell Cathodes.*Int. J. Hydrogen Energ.* **2009**,*34***,** 3104-3111.
https://doi.org/10.1016/j.ijhydene.2009.01.022

[21] Klages, M.; Enz, S.; Markötter, H.;Manke, I.; Kardjilov, N.; Scholta, J.Investigations on Dynamic Water Transport Characteristics in Flow Field Channels Using Neutron Imaging Techniques.*J. Power Sources***2013**, *239*, 596-603.
https://doi.org/10.1016/j.jpowsour.2013.01.196

[22] Norouzi, N.;Talebi, S.An Overview on the Green Petroleum Production.*Chem. Rev. Lett.* **2020**,*3*, 38-52.
https://doi.org/10.22034/crl.2020.222515.1041

[23] Norouzi, N.;Fani, M.;Ziarani, Z.K. The Fall of Oil Age:A Scenario Planning Approach over the Last Peak Oil of Human History by 2040.*J. Petrol. Sci. Eng.* **2020**,*188*, 106827.
https://doi.org/10.1016/j.petrol.2019.106827

[24] Mirvakili, A.; Chahibakhsh, S.;Ebrahimzadehsarvestani, M.; Soroush, E.;Rahimpour, M.R. Modeling and Assessment of Novel Configurations to Enhance Methanol Production in Industrial Mega-Methanol Synthesis Plant. J. *Taiwan Inst. Chem. Eng.* **2019**,*104*, 40-53. https://doi.org/10.1016/j.jtice.2019.09.018

[25] Chen, K.; Yu, J.; Liu, B.; Si, C.; Ban, H.; Cai, W.; Li, C.; Li, Z.; Fujimoto, K.Simple Strategy Synthesizing Stable CuZnO/SiO$_2$ Methanol Synthesis Catalyst.*J. Catal.* **2019**,*372*, 163-173.https://doi.org/10.1016/j.jcat.2019.02.035

**ОБЧИСЛЮВАЛЬНА МОДЕЛЬ
ДЛЯ ПРОГНОЗУВАННЯ КОРИСНОЇ
ПОТУЖНОСТІ ПАЛИВНОГО ЕЛЕМЕНТУ
ПРОТОНООБМІННОЇ МЕМБРАНИ**

Анотація*. Показано збільшення електричної енергії внаслідок збагачення киснем. З метою максималізації кількості кисню у всіх областях каталітичного шару (CL), для питомої ефективної площі мембрани (МЕА) змодельовано поле потоку (FF). За розробленою моделлю 3DCFD спрогнозована швидкість приросту електричної енергії за підвищення кількості кисню в CL на 1 %. Змодельовано зволожену повітряну суміш на паливному елементі протонообмінної мембрани (PEMFC). Показано, що аналітичні та розрахунковий гідродинамічний метод дають подібні результати, а похибка моделі CFD становить приблизно 1,9 % порівняно з аналітичним методом.*

Ключові слова*: обчислювальна гідродинаміка, модель поля потоку, паливний елемент, аналіз ефективності.*